Environmental Science & Technology

pubs.acs.org/est

Article

Thin-Film Composite Membranes for Hydrogen Evolution with a Saline Catholyte Water Feed

Le Shi,* Xuechen Zhou, Rachel F. Taylor, Chenghan Xie, Bin Bian, Derek M. Hall, Ruggero Rossi, Michael A. Hickner, Christopher A. Gorski, and Bruce E. Logan*

Cite This: *Environ. Sci. Technol.* 2024, 58, 1131−1141

Read Online

ACCESS | Metrics & More | Article Recommendations | Supporting Information

ABSTRACT: Hydrogen gas evolution using an impure or saline water feed is a promising strategy to reduce overall energy consumption and investment costs for on-site, large-scale production using renewable energy sources. The chlorine evolution reaction is one of the biggest concerns in hydrogen evolution with impure water feeds. The "alkaline design criterion" in impure water electrolysis was examined here because water oxidation catalysts can exhibit a larger kinetic overpotential without interfering chlorine chemistry under alkaline conditions. Here, we demonstrated that relatively inexpensive thin-film composite (TFC) membranes, currently used for high-pressure reverse osmosis (RO) desalination applications, can have much higher rejection of Cl^- (total crossover of 2.9 ± 0.9 mmol) than an anion-exchange membrane (AEM) (51.8 ± 2.3 mmol) with electrolytes of 0.5 M KOH for the anolyte and 0.5 M NaCl for the catholyte with a constant current (100 mA/cm^2 for 20 h). The membrane resistances, which were similar for the TFC membrane and the AEM based on electrochemical impedance spectroscopy (EIS) and Ohm's law methods, could be further reduced by increasing the electrolyte concentration or removal of the structural polyester supporting layer (TFC-no PET). TFC membranes could enable pressurized gas production, as this membrane was demonstrated to be mechanically stable with no change in permeate flux at 35 bar. These results show that TFC membranes provide a novel pathway for producing green hydrogen with a saline water feed at elevated pressures compared to systems using AEMs or porous diaphragms.

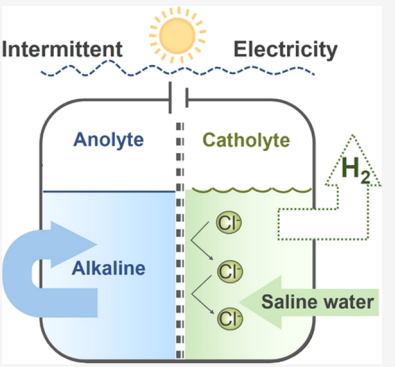

KEYWORDS: *green hydrogen evolution, water electrolyzer, saline water, thin-film composite membrane, ion transport control*

INTRODUCTION

Hydrogen gas (H_2) is one of the most promising energy carriers to store multi-gigawatt levels of electrical energy generated from intermittent renewable energy sources due to its high energy density (120−142 MJ/kg).[1,2] Producing H_2 by water electrolysis has been considered as a bridging technology between abundant, but intermittent, renewable electrical energy and chemical energy[3] because of its potentially low pollution impact, fast production rate, mild reaction conditions, and high purity (>99.999%).[4,5] Researchers have focused on making this process more energy-efficient and economical because the costs for producing H_2 by water electrolysis can be two to four times higher than conventional methods using natural gas.[6,7] Although the capital costs for water electrolyzer stacks vary, the membrane and catalysts can account for 25−50% of the total.[8,9]

High purity water feeds are currently required for all commercial water electrolyzers, which necessitate the use of supporting ancillary components like extensive water purification systems.[10] Although several techno-economic studies have been published in the past several years,[11,12] a more comprehensive review with up-to-date costs is still needed and the cost of water purification systems remains significant especially for on-site hydrogen production.[13−15] Among various water electrolysis technologies, alkaline water electrolyzers (AWEs) are readily available, durable, and have higher tolerance of impurities especially for chloride.[16−19] The "alkaline design criterion" for impure water electrolysis is being used by many researchers because water oxidation catalysts can exhibit larger kinetic overpotentials without driving chlorine redox chemistry under alkaline conditions.[20]

Traditional AWEs use thick (2−3 mm), porous diaphragms as separators, which contribute a large Ohmic loss resulting in high overpotentials at high current densities.[21] Their highly porous structure requires highly concentrated potassium hydroxide (KOH, 20% to 30 wt %) electrolytes to provide stable ionic conductivity.[16,22] AWEs with porous diaphragms also require balanced pressure operation (between the catholyte and anolyte), as a large differential pressure can produce extensive crossover of the electrolytes and dissolved gas products which may result in explosion hazards.[23] AWEs

Received: September 25, 2023
Revised: December 20, 2023
Accepted: December 21, 2023
Published: January 3, 2024

using anion-exchange membranes (AEMs) as separators theoretically do not need alkaline electrolytes and can have low gas crossover. However, there are a few reports on AEMs being used commercially with deionized water instead of liquid aqueous KOH due to AEMs' insufficient conductivity and stability compared to liquid basic electrolytes.[3,19,24−26]

Thin-film composite (TFC) membranes have recently been shown to perform comparably to ion-exchange membranes with a supporting electrolyte in electrochemical energy conversion systems.[27] Combining an ultrathin selective layer with a highly porous substrate, they serve as an alternative separator that could potentially overcome the trade-off between conductivity and selectivity.[3,27] These membranes are much thinner than traditional porous diaphragms which do not require highly concentrated supporting electrolyte and much less expensive than ion-exchange membranes.[3,28] One type of TFC membrane, originally developed for use in reverse osmosis (RO) desalination of seawater, was recently shown to have performance similar to that of a cation-exchange membrane (CEM) for hydrogen gas production with a synthetic seawater catholyte. The overpotential at a constant current density of 10−40 mA/cm^2 in an asymmetric seawater electrolyzer using a contained anolyte (1 M $NaClO_4$) that cannot be oxidized at the anode in order to favor the oxygen evolution reaction (OER), and a NaCl catholyte (1 M) had an overpotential similar to that of a CEM in the same system.[29,30] The active layer of the TFC membrane retained larger hydrated salt ions but allowed the transport of smaller water ions (protons and hydroxide ions) to balance the charge. Therefore, the ability of these TFC membranes to efficiently transport protons or hydroxide ions and reject larger salt ions makes them a promising option for use in AWEs especially in the presence of impurities in the electrolytes. The chemical stability of TFC membranes is also important for long-term use, which is highly dependent on their polymer composites and the exposure to conditions out of the specified pH range for limited periods of time, such as several weeks, appears to be possible.[31−33] In addition, methods are being developed to produce TFC membranes that are highly stable under alkaline conditions, for example, by using polyethylenimine (PEI) cross-linked with triglycidyl isocyanurate (TGIC).[33]

In this work, we investigated the performance of a TFC membrane (BW30XLE) under alkaline and near-neutral pH solution conditions in symmetric and asymmetric AWEs. Non-noble metal nickel foam-based anodes (S-(Ni, Fe)OOH) were used because they provide a highly porous electrode structure that can achieve good transport of electrons, ions, and water on the surface of catalysts, as well as gases to avoid blockage by bubbles.[16] There are also nonprecious metal cathode catalysts that can be used for the hydrogen evolution reaction under highly alkaline conditions.[34,35] However, a Pt catalyst (10% Pt/C) was used here for convenience and to provide the same cathode conditions for both neutral pH and highly alkaline electrolyte conditions.[36] The membrane resistance was measured under different electrolyte conditions with two methods (an Ohm's law approach and an electrochemical impedance spectra approach) for a better understanding of membrane surface properties. The resistance of the TFC membrane was examined with its unmodified three-layer structure containing a thin polyamide active layer, a polysulfone support layer, and a polyester (PET) nonwoven fabric support layer. The TFC membrane was also examined following the removal of the PET layer (TFC-no PET) which is only needed for very high RO pressures (~80 bar)[37] to determine the contribution of this thick layer to the membrane resistance. The performance of AWEs with TFC-no PET membranes was examined based on their overpotentials at constant current densities in symmetric and asymmetric alkaline electrolytes. The ion transport selectivity was further evaluated in asymmetric electrolytes with alkaline anolytes and Cl^- present in catholyte. A defined saline catholyte (NaCl) was used to simplify the monitoring of ion crossover, focusing on the most important component of impure water. The ion transport stability of TFC-no PET membranes was examined based on the change in the ion diffusion rate change over time after operating in AWEs. The mechanical stability of the TFC-no PET membrane was also examined by monitoring any changes in permeate flux change with applied pressure using a dead-end filtration setup.

EXPERIMENTAL SECTION

Chemicals and Materials. Iron(III) nitrate nonahydrate ($Fe(NO_3)_3·9H_2O$, 98%, Sigma-Aldrich), sodium thiosulfate pentahydrate ($Na_2S_2O_3·5H_2O$, J.T. Baker), hydrochloric acid (36.5−38%, VWR), ethanol (200 proof, KOPTEC), Nafion perfluorinated resin solution (5 wt %, Sigma-Aldrich), sodium chloride (NaCl, Sigma-Aldrich), potassium hydroxide (KOH, Sigma-Aldrich), sodium perchlorate ($NaClO_4$, Sigma-Aldrich), sucrose ($C_{12}H_{22}O_{11}$, 99%, Thermo Scientific), and Pt/C (10 wt %, Fuel Cell) were used as received. Ni foam (with the thickness of 1.6 mm, the porosity of 350 g/m^2) and carbon cloth (with the thickness of 0.356 mm, the density of 1.5 g/cm^3, AvCarb 1071 HCB, AvCarb Material Solutions) were used as the electrode substrates. Deionized (DI) water (>18.3 MΩ·cm at room temperature) was used for the preparation of all aqueous solutions. The membranes were an anion-exchange membrane (AEM, 106 ± 1 μm thick with an ion-exchange capacity of 1.85 mmol/g, Selemion AMV, Asashi Glass) and polyamide-based thin-film composite (TFC) membranes for brackish water desalination (RO, BW30XLE, Dupont).

Electrode Preparation. The porous S-(Ni, Fe)OOH catalysts were prepared on Ni foam with a simple one-step solution-phase method as previously reported.[35] Ni foam (2 × 2 cm^2) was cleaned with HCl (2 M) in an ultrasound bath for 10 min to remove the surface oxide layer and then sonicated in DI water and ethanol for 10 min each to remove the extra acid. The precursor of $Fe(NO_3)_3·9H_2O$ (0.35 g) and $Na_2S_2O_3·5H_2O$ (0.05 g) was dissolved in 10 mL of DI water for one piece of Ni foam. Each Ni foam was placed in a small beaker of precursor with shaking for 5 min, and the color of the Ni foam changed from its original metallic color to a dark black (Figure S1). The samples were then washed several times with DI water and dried in air.

Cathodes were made using 10% Pt/C coated on carbon cloth with a brush as previously reported.[38] Carbon cloth (2 × 2 cm^2) was first cleaned with HCl (2 M) in an ultrasound bath for 10 min and then sonicated in DI water and ethanol for 10 min each. Then, the carbon cloth was moved to a muffle oven (450 °C) overnight. The precursor of 10% Pt/C powder (40 mg), Nafion ionomer (6.67 μL), isopropanol (3.33 μL), and DI water (0.83 μL) for one piece of carbon cloth was mixed by vortexing and then transferred into an ultrasound bath for 1 h. The pastelike precursor was then painted on the carbon cloth using a paintbrush. The prepared samples were then dried in air overnight.

https://doi.org/10.1021/acs.est.3c07957
Environ. Sci. Technol. 2024, 58, 1131−1141

Membrane Pretreatment and Resistance Measurements. Before testing, TFC membranes were pretreated in a 25% isopropanol solution for 30 min in a rotating shaker, followed by rinsing with DI water and shaking for three 30 min cycles. Then, the polyester (PET) nonwoven layers were carefully removed by peeling them away from the other layers (polysulfone and polyamide) of each membrane. The pretreated membrane noted as TFC-no PET was stored in DI water for further use (Figure S2).

The ionic resistances of membranes were measured using two different methods at room temperature: an Ohm's Law approach and an electrochemical impedance spectroscopy (EIS) approach (Figure S3). The membrane was placed in a custom-fabricated cell. Each chamber and the Luggin capillary tube were filled with the same solution (KOH, 0.5 or 2 M). For the Ohm's Law, the exposed membrane area was fixed with a gasket to produce an exposed area the same as the reactor cross section (7 cm^2). Two platinum-coated titanium mesh electrodes (4.4 cm^2) were placed at each end of the chamber (10 cm apart). Two Ag/AgCl reference electrodes were placed into each one of the Luggin capillary tubes, of which the end tip was around 2 mm apart from the membrane surface.[30] Direct current (over a range of 0.06−0.6 mA/cm^2) was applied with and without the membrane, and the potential drop was monitored. For the EIS approach, an alternating current (a frequency range of 500 kHz to 10 Hz with a signal amplitude of 10 mV) was applied with and without the membrane. The resistance of the membrane (R_m) was determined by subtracting the resistance measured without membranes (R_{sol}) from the resistance measured with membranes (R_{m+sol}). The interfacial layer resistance of each membrane can be calculated from the difference between these two methods.[39,40] All measurements were made in triplicate, and the data were reported as the average of the measurements, and the standard deviation gave the error bars.

Electrochemical Measurements. All electrochemical tests were conducted at room temperature using a potentiostat (VMP3, Bio-Logic). A three-electrode system was used to separately monitor the hydrogen evolution reaction (HER) and oxygen evolution reaction (OER). The system contained a 10% Pt/C coated carbon cloth or S-(Ni, Fe)OOH/Ni foam as the working electrode, a graphite rod counter electrode, and a reference electrode of Hg/HgO (in 1 M NaOH) for alkaline electrolytes. Electrolytes with five concentrations (0.25, 0.5, 1.0, 2.0, and 4.0 M) were used for each electrode. All measured potentials vs Hg/HgO were converted to a reversible hydrogen electrode (RHE) by E_{RHE} (V) = $E_{Hg/HgO}$ + 0.0591 pH + 0.098. Linear sweep voltammetry (LSV) for HER was carried out at 5 mV/s between 0.4 and −0.4 V (vs RHE) in the KOH electrolyte. For studying the OER reaction, LSV tests were carried out between 0 V (vs OCV) and 1.6 V (vs RHE) in the KOH electrolyte.

The stability of the S-(Ni, Fe)OOH/Ni foam electrode was investigated with chronopotentiometry (CP) at a constant current density of 100 mA/cm^2 for 48 h in a 0.5 M KOH electrolyte in a three-electrode system. The stabilities of both S-(Ni, Fe)OOH/Ni foam and 10% Pt/C electrodes were examined in a two-electrode system in 0.5 M KOH electrolyte at a constant current for three cycles with each cycle of 40 mA/cm^2 for 10 h and 150 mA/cm^2 for 10 h. EIS was obtained at OCV from 100 kHz to 100 mHz with an amplitude of 10 mV.

Electrolyzer Cell Assembly and Operation. The electrolyzer cell was assembled using an anode of S-(Ni, Fe)OOH/Ni foam (2 × 2 cm^2) on a platinized Ti plate, a membrane, and a cathode of 10% Pt/C carbon cloth (2 × 2 cm^2) on a graphite plate with serpentine flow fields (Scribner Associate Inc.) that was tightened with a torque wrench to 9 N m (Figure S4). Before the electrolyzer was assembled, the S-(Ni, Fe)OOH/Ni foam was pressed, and a fabric spacer mesh (60 μm thick and 25% porosity; Sefar Nitex, 07−40/25) was placed between the S-(Ni, Fe)OOH/Ni foam and the membrane to introduce a small gap to avoid piercing the membrane during assembly. The additional small gap between the electrode and membrane has been reported to strongly reduce the overpotential relating to gas bubbles[41] and reduce the gas crossover.[17] This configuration has been referred to as near-zero gap.[41,42] The TFC-no PET membrane was placed with the active layer facing the catholyte in all of the experiments. The system was carried out using Teflon tubing and HDPE electrolyte reservoirs to avoid glass-corrosion-induced contaminants using alkaline solutions. Anolyte was 1 L of KOH (0.5 or 2.0 M), and the catholyte was 1 L of KOH (0.5 M) for different conditions as noted in the figures. The flow rate of catholyte and anolyte in each chamber was controlled at 15 mL/min for electrolyzer tests using a peristaltic pump. LSV was carried out at 5 mV/s between 0 and 2.4 V.

To analyze the overpotential distribution in the electrolyzer, a reference electrode (Hg/HgO and 1 M NaOH) was added to the inlet of the anode chamber in the electrolyzer (Figure S5). The anode potential and cathode potential were recorded using CP with current densities applied (10, 20, 40, 80, 100, 200, 400 mA/cm^2) for 30 min in each step and 100 mA/cm^2 for 20 h. High frequency resistance (R) from EIS was recorded in a two-electrode system with the same CP current (i) under each condition for the internal overpotential calculation. The anodic overpotential (η_{OER}) was calculated based on the difference between the theoretical OER potential (E_{OER}^0 = 1.23 V vs RHE) and the recorded working potential (E_w vs RHE): $\eta_{OER} = E_w - E_{OER}^0$. The overpotential related to membranes was calculated by $\eta_{mem} = iR$. The cathodic overpotential (η_{HER}) was calculated based on the difference between the theoretical HER potential (E_{HER}^0 = 0 V vs RHE) and the recorded counter potential (E_c vs RHE) minus the membrane overpotential (η_{mem}): $\eta_{HER} = -(E_c - \eta_{mem} - E_{HER}^0)$.

Ion Crossover Measurements. To monitor the ion crossover across each membrane under different conditions, asymmetric solutions were used as electrolytes. The two-electrode system was used to apply a constant current density (100 mA/cm^2) between the anode and cathode for 20 h. The catholyte and anolyte solutions were collected and diluted to measure salt ion concentrations using ion chromatography (IC, Dionex ICS-1100, Thermo Scientific). All of the measurements were conducted at least three times with different pieces of membrane.

Membrane Stability Test. Ion transport stability of membranes before and after the electrolyzer test (with a constant current of 100 mA/cm^2 applied for 10 and 20 h under different conditions) was monitored by conducting a salt diffusion measurement using the electrolyzer flow cell. A solution of 0.5 M NaCl was circulated into the chamber facing the back layer of the TFC-no PET membrane. A solution of 0.9 M sucrose was used to balance the osmotic pressure circulated into the chamber facing the active layer of the TFC-no PET membrane. The rate of salt diffusion through the

https://doi.org/10.1021/acs.est.3c07957
Environ. Sci. Technol. 2024, 58, 1131−1141

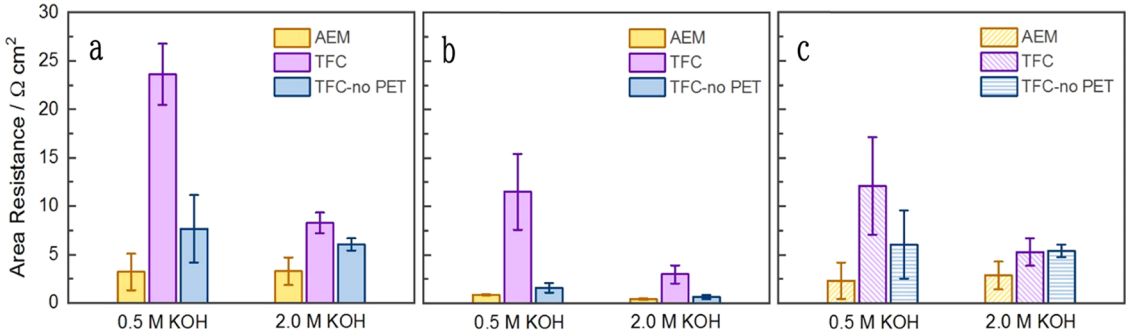

Figure 1. Membrane (AEM, TFC, and TFC-no PET) resistances under different electrolyte conditions (0.5 M KOH and 2.0 M KOH) measured in a four-electrode lab-made cell using (a) Ohm's law approach or (b) the EIS approach. (c) Interfacial layer resistance of different membranes at each condition.

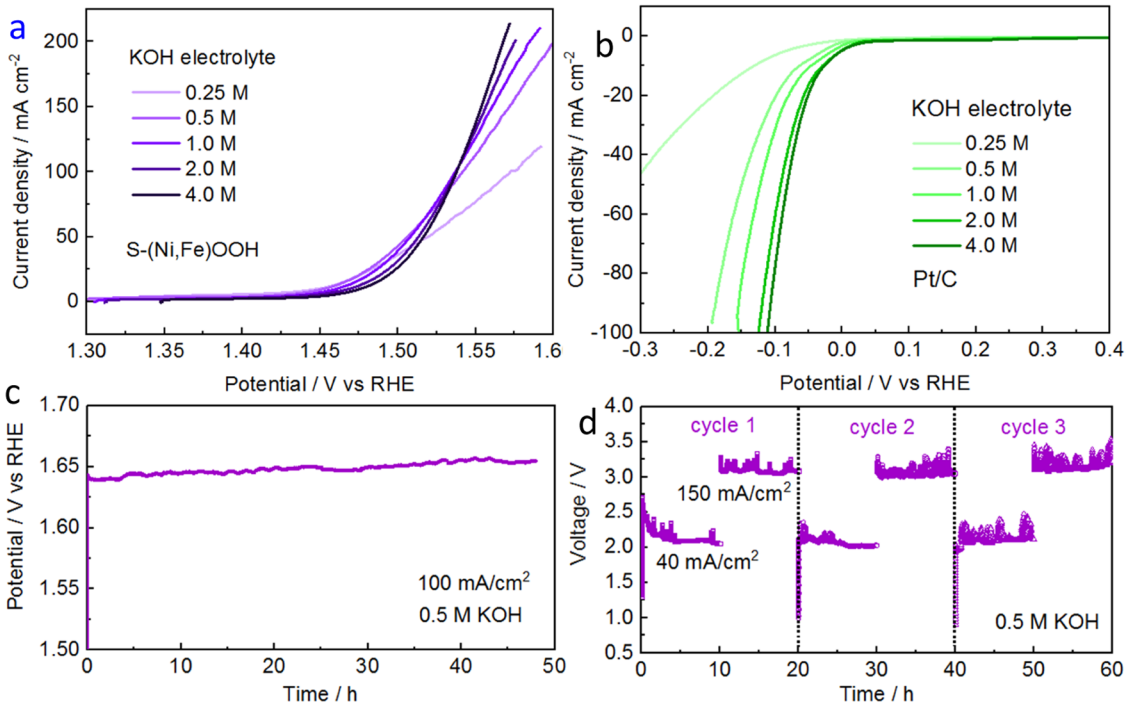

Figure 2. LSV measurements in KOH alkaline electrolytes of different concentrations for (a) the OER with the S-(Ni, Fe)OOH electrode and (b) the HER with the Pt/C electrode. LSV results are presented with *iR* correction. Stability test in 0.5 M KOH electrolyte for (c) the S-(Ni, Fe)OOH electrode at a constant current density of 100 mA/cm^2 for 48 h in a three-electrode system and (d) both the S-(Ni, Fe)OOH and the Pt/C electrodes at a constant current for 60 h in three cycles with each cycle of 40 mA/cm^2 for 10 h and 150 mA/cm^2 for 10 h in a two-electrode system. Stability results are presented without *iR* correction.

membrane was obtained by using a pair of flow-through conductivity electrodes (ET908 Flow-Thru Conductivity Electrode, eDAQ) located at each outlet. The conductivity change in the sucrose chamber was converted to a NaCl concentration by using a linear calibration curve (Figure S6). TFC membranes can degrade over time when exposed to highly alkaline solutions.[32] To ensure that the membrane integrity was stable during all tests conducted here, the overpotential was monitored over a period of 72 h using the 2.0 M KOH anolyte and 0.5 M KOH catholyte, a period of time consistent with other stability studies.[34,35,39]

The integrity of the TFC-no PET membrane under high pressure was examined in an HP4750 dead-end filtration cell (Sterlitech) with a 14.6 cm^2 filtration area without stirring. A coupon of TFC-no PET membrane was supported by the addition of mesh (60 μm thick and 25% porosity; Sefar Nitex, 07−40/25) between the membrane and support disk to simulate the near-zero-gap condition in the electrolyzer. Ultrapure water (UPW, Elga PURELAB Flex 3) was used as the feed and filtered at constant applied pressures from 100 to 500 psi at room temperature. Permeate mass was measured continuously using an FX-200i balance (A&D Company) and recorded automatically every five seconds via RsWeight software.

RESULTS AND DISCUSSION

Membrane Resistance in Different Electrolytes. TFC membranes with the PET layer removed had a resistance comparable to that of AEM with an increasing concentration of KOH electrolytes. The membrane resistance using Ohm's law was reduced from 23.6 ± 3.2 Ω cm^2 (TFC) to 7.7 ± 3.5 Ω cm^2 in 0.5 M KOH solution after removing the PET layer (TFC-no PET) which is only needed for very high pressures. Increasing the concentration of the electrolyte to 2 M KOH further

https://doi.org/10.1021/acs.est.3c07957
Environ. Sci. Technol. 2024, 58, 1131−1141

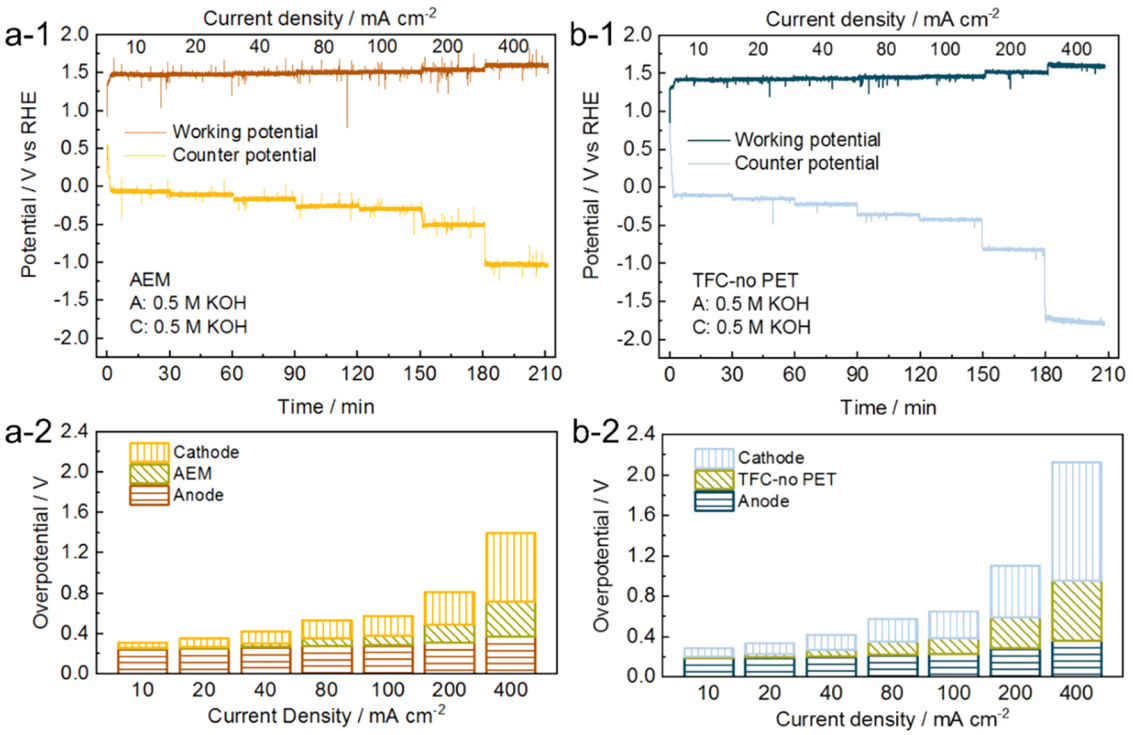

Figure 3. Overpotential contribution analysis for alkaline water electrolyzer with S-(Ni, Fe)OOH and 10% Pt/C electrodes using (a) AEM and (b) TFC-no PET as separators. Step constant current density was applied (10, 20, 40, 80, 100, 200, and 400 mA/cm^2) for 30 min/step (without *iR* correction). (1) The potential of working and counter electrodes was recorded using Hg/HgO reference electrode. (2) The membrane overpotential is calculated by applied current times the membrane resistance from EIS measurement at each step in a two-electrode system.

reduced the TFC-no PET resistance to 6.1 ± 0.6 Ω cm^2, which was higher than that of the AEM (3.3 ± 1.4 Ω cm^2) (Figure 1a). When calculating the membrane resistance using Ohm's law approach with direct current, the membrane and interfacial layer resistances cannot be separated.[40] Therefore, EIS was used to measure the interfacial layer resistances due to the electrical double layer and the diffusion boundary layer.[40,43] The resistance of TFC-no PET membrane based on EIS was 1.6 ± 0.5 Ω cm^2 in 0.5 M KOH and 0.6 ± 0.2 Ω cm^2 in 2 M KOH. These resistances were slightly larger than that of an AEM membrane in 0.5 M KOH (0.87 ± 0.06 Ω cm^2) and in 2.0 M KOH (0.42 ± 0.09 Ω cm^2) (Figure 1b).

Both the double layer and the diffusion boundary layer will hinder ion transport, especially under conditions with low salt concentrations.[40] Increasing the solution concentration could reduce the thickness of the double layer and diffusion boundary layer due to the higher screening effect of the attractive electrical interactions between the counterions and surface charge of the membrane.[44] Therefore, the difference in resistance between Ohm's law and EIS resistance measurement approaches was more pronounced at lower salt concentrations (Figure 1c). The measured resistance decreased with increasing salt concentration especially for the TFC membrane, while the resistance of AEM and TFC-no PET showed less decrease with increasing salt concentration, which indicated that the PET layer required a high concentration of the electrolyte to reduce resistances similar to a porous diaphragm.[3]

Electrode Overpotentials and Stability in AWE. To assess the electrocatalytic performance of the prepared electrodes under different electrolyte conditions, we first investigated the OER activity of S-(Ni, Fe)OOH electrodes in KOH electrolytes with different concentrations (Figure 2a). The overpotential for the OER with the S-(Ni, Fe)OOH electrode at a current density of 100 mA/cm^2 was reduced from 340 mV (0.25 M KOH) to 310 mV by increasing the KOH concentration to 0.5 M. As the concentration of KOH was further increased to 4.0 M, the overpotential required at 100 mA/cm^2 was only marginally decreased to 300 mV. The HER activity of 10% Pt/C electrodes was also investigated in alkaline conditions with KOH electrolytes across different concentrations (Figure 2b). The overpotential for a 10% Pt/C electrode at the current density of 100 mA/cm^2 was reduced from >400 mV (0.25 M KOH) to 196 mV by increasing the KOH concentration to 0.5 M. The overpotential was further reduced to 113 mV when the KOH concentration increased to 4.0 M. The mechanism for this enhancement is still being debated because the concentration of hydronium ions is too low for these currents in concentrated alkaline electrolytes and water molecules to become the main reactant.[45] The enhanced performance of HER activity in a higher concentration of alkaline solution might be due to the hydronium ions intermediates generated from H_2O dissociation in high pH electrolytes on the surface of nanostructured Pt/C.[46] The effects of electrolyte conductivity were excluded by using *iR* correction (Figure S7).

Both the S-(Ni, Fe)OOH anode and 10% Pt/C cathode demonstrated good operational durability in 0.5 M KOH alkaline solution. Under a constant current density of 100 mA/cm^2, the measured voltage of OER using S-(Ni, Fe)OOH electrode remained highly stable with only a slight change of 3.11 × 10^{-4} V/h over 48 h (Figure 2c). The good durability mainly originated from the robust contact between the S-(Ni, Fe)OOH layer and the Ni foam substrate, as well as the excellent corrosion resistance of the metal (oxy)hydroxide.[34] The water splitting performance also showed good durability at

https://doi.org/10.1021/acs.est.3c07957
Environ. Sci. Technol. 2024, 58, 1131−1141

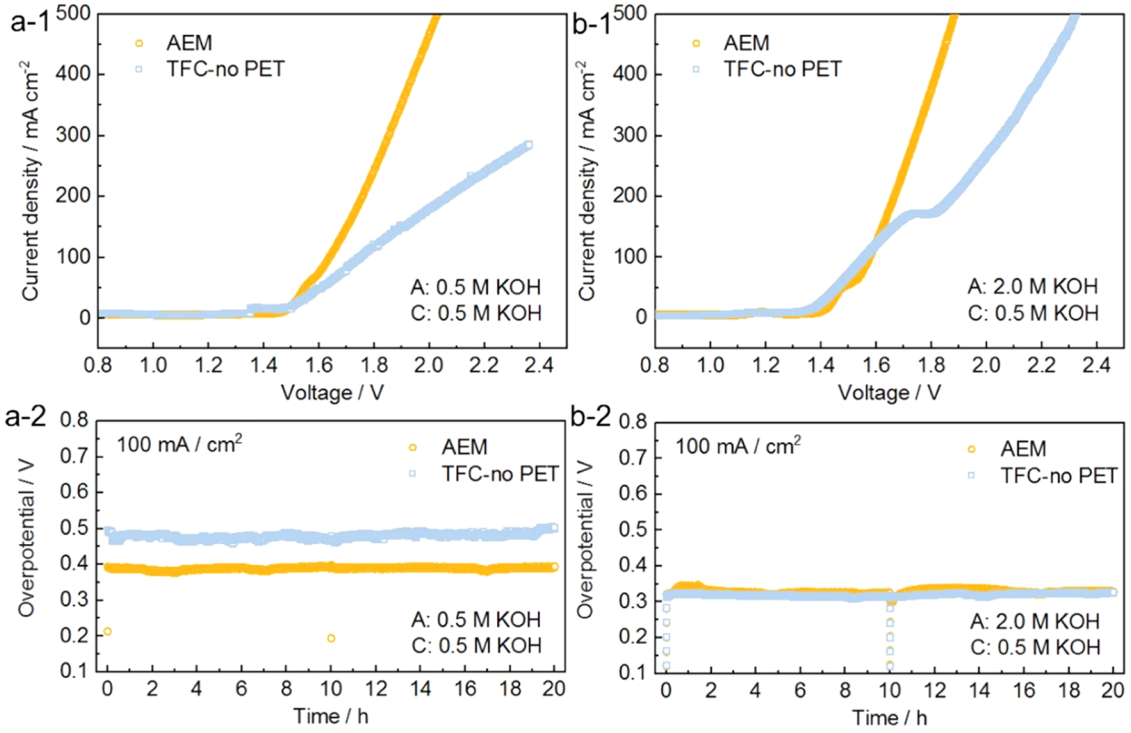

Figure 4. Electrochemical performance measurement for an alkaline water electrolyzer with AEM and TFC-no PET membranes in (a) symmetric 0.5 M KOH anolyte and 0.5 M KOH catholyte and (b) asymmetric 2.0 M KOH anolyte and 0.5 M KOH catholyte. (1) LSV measurement with a scan rate of 5 mV/s and (2) overpotential measurement by CP with applied constant current density of 100 mA/cm^2 for 20 h. All of the data are presented with *iR* correction.

a constant current density for 60 h in three cycles with each cycle of 40 mA/cm^2 for 10 h and 150 mA/cm^2 for 10 h (Figure 2d). Fluctuations in the voltage were likely due to gas bubbles generated on the electrode surface inducing undesired overpotentials.[47]

Overpotential Contribution Analysis in AWE. To assess the relative impact of the membrane resistance on AWE performance, the electrode overpotentials were calculated and compared to those of the membrane. The overpotentials increased with the current density for both AEM and TFC-no PET membranes. The overpotential required to operate the AWE at 100 mA/cm^2 was 0.652 V for TFC-no PET, which was only 74 mV higher than AWE with AEM (0.578 V), which indicated that using the TFC-no PET membrane only added a small overpotential to the whole system (Figure 3a1,b1). The use of TFC-no PET contributed 24% to the total overpotential, while the AEM contributed 16% to the total overpotential at the applied current density of 100 mA/cm^2, which indicated that the overpotential contribution from membranes was a small portion of the total overpotential compared to the overpotential contribution from anode and cathode (Figure 3a2,b2).

The overpotentials of S-(Ni, Fe)OOH anodes in both configurations were similar, with an increase from 0.191 V (10 mA/cm^2) to 0.366 V (400 mA/cm^2) for the TFC-no PET membrane and from 0.251 V (10 mA/cm^2) to 0.373 V (400 mA/cm^2) for the AEM. The S-(Ni, Fe)OOH anode overpotential in 0.5 M KOH alkaline electrolyte measured here was consistent with the recent reports on state-of-the-art performance for alkaline OER.[35] The overpotentials of 10% Pt/C cathodes in the configuration with the TFC-no PET membrane increased more significantly than that in the configuration with AEM as the applied current increased. The cathode overpotential using TFC-no PET membrane increased from 0.080 V (at 10 mA/cm^2) to 0.261 V (at 100 mA/cm^2), while the cathode overpotential using AEM increased from 0.054 V (at 10 mA/cm^2) to 0.202 V (at 100 mA/cm^2). Therefore, despite a higher operating voltage being required than using AEM in AWE, using a less expensive TFC-no PET membrane in AWE could decrease the capital costs for green hydrogen production and the overpotential could be controlled at a certain current range.[7]

Asymmetric Electrolyte Effects in AWE. The AWE overpotential of the system with the TFC-no PET membrane was further reduced by using a more concentrated alkaline anolyte to compensate for electro-osmotic water flux. In tests using the TFC-no PET membrane and both electrolytes containing 0.5 M KOH (100 mA/cm^2 over 20 h), it was observed that the catholyte volume increased and the anolyte volume decreased with a volume change of 100 ± 10 mL. Because there was no difference in osmotic pressure between the two electrolyte chambers (23.5 bar for each chamber, Table S1) and the water consumed due to water splitting was negligible at this condition (2.68 mL, SI), the observed flux was concluded to be due to electro-osmotic flow. The electro-osmotic flow was likely associated with the crossover of K^+ ions driven by the electric field and the surface negative charge on the TFC membrane. Water molecules associated with OH^- ions would have moved water in the other direction (from the cathode to anode).[48] Under alkaline conditions, water splitting proceeds through an oxidation reaction of $2OH^- \rightarrow 2e^- + 1/2\ O_2 + H_2O$ and a reduction reaction of $2H_2O + 2e^- \rightarrow 2OH^- + H_2$. For the oxidation reaction to proceed at a steady state, OH^- ions have to be transported from the cathode to the anode through the membrane. A limiting current can arise when OH^- ions are consumed at the anode faster than they are

https://doi.org/10.1021/acs.est.3c07957
Environ. Sci. Technol. 2024, 58, 1131−1141

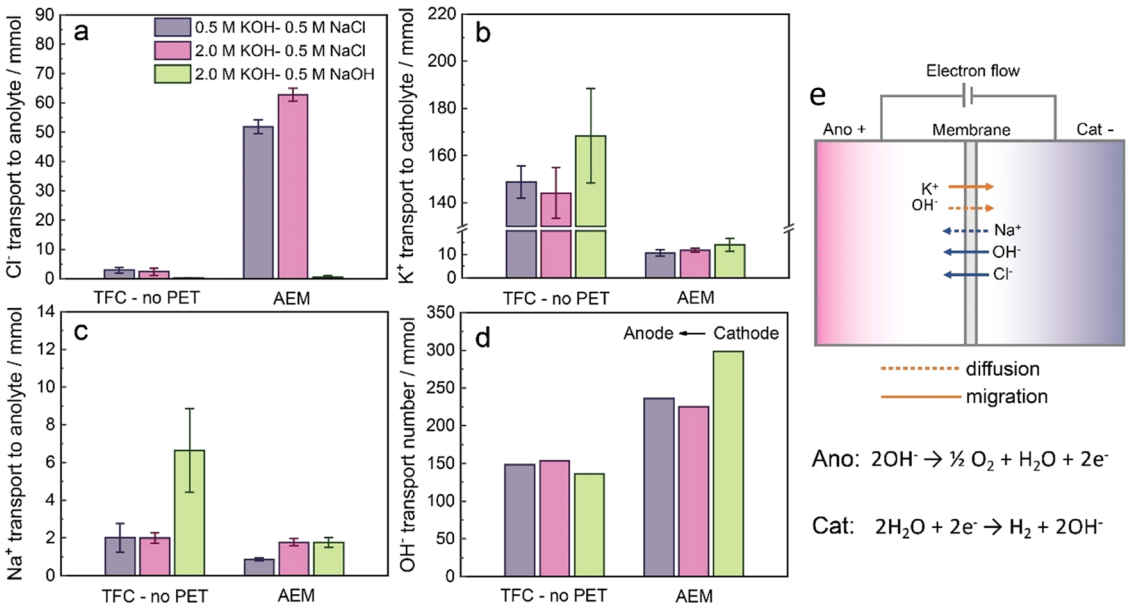

Figure 5. Amount number of cations and anions crossover in catholyte and anolyte reservoir using different membranes after applying a constant current of 100 mA/cm^2 for 20 h: (a) Cl^- transport from catholyte to anolyte, (b) K^+ transport from anolyte to catholyte, (c) Na^+ transport from catholyte to anolyte, and (d) OH^- transport calculated based on the constant current conditions and the other ion crossover amount. (e) Schematic figure showing ions moving under constant current, with the solid line indicating the migration process and the dotted line indicating the diffusion process.

transported through the membrane.[49,50] When the anolyte concentration was increased to 2.0 M KOH (0.5 M KOH catholyte) to provide an osmotic pressure to drive water from the catholyte to compensate for the electro-osmotic flow, the overpotential using the TFC-no PET was reduced from 0.48 V (0.5 M KOH anolyte and 0.5 M KOH catholyte) to 0.32 V (Figure 4). The overpotential using the AEM was also changed, but only slightly by using the same concentrations of KOH (0.5 M) in both chambers (0.38 V) compared to a slightly lower overpotential using the 2 M anolyte (0.32 V) at the same current condition of 100 mA/cm^2 (Figure 4).

Increasing the KOH anolyte concentration from 0.5 to 2 M increased the osmotic pressure of anolyte from 23.5 to 111 bar (Table S1). This osmotic pressure difference built a driving force for water flow from the catholyte to the anolyte, which partially compensated for electro-osmotic water flow from the anolyte to the catholyte. This suggests that the electro-osmotic drag due to OH^- transport from the catholyte to the anolyte partially offset the electro-osmotic flow due to the K^+ crossover from anolyte to catholyte. The counter flow of water due to the difference in osmotic pressure was consistent with our observations that using the 2 M anolyte avoided a change in electrolyte volume, and the overpotential of the TFC-no PET membrane after *iR* correction (0.32 V) was the same as that of the AEM (0.32 V) at a current density of 100 mA/cm^2 (Figures 4b and S8). Monitoring the time rate of the electrolyte volume change over time would be helpful in the future to examine changes in the drop in potential drop on the membrane and electro-osmotic flow velocity.[51]

Ion Crossover in AWE with the TFC Membrane. Ion transport mechanism was evaluated using different types of asymmetric electrolytes. The ion crossover under different conditions was analyzed for both AEM and TFC-no PET membranes after 20 h under a constant current of 100 mA/cm^2. For the TFC-no PET membrane, the Cl^- crossover amount was only 2.9 ± 0.9 mmol with the electrolytes of 0.5 M KOH anolyte and 0.5 M NaCl catholyte and 2.3 ± 1.2 mmol with the electrolytes of 2.0 M KOH anolyte and 0.5 M NaCl catholyte (Figure 5a). Cl^- crossover using the AEM was much larger with 51.8 ± 2.3 mmol in 0.5 M KOH anolyte and 0.5 M NaCl catholyte and 62.8 ± 2.2 mmol in 2.0 M KOH anolyte and 0.5 M NaCl catholyte (Figure 5a). These results indicate that the electrolyzers with TFC membranes can be used to successfully contain salt ions in the individual electrolytes, unlike ion-exchange membranes that facilitate selective transport of either cations or anions. This ability of the TFC membrane to retain both of the salt ions makes them particularly useful for using unconventional water sources such as seawater catholytes or other impure water sources.[29]

The larger crossover of K^+ in TFC-no PET than in AEM (Figure 5b) was likely due to the weaker electrostatic repulsion effects for cations, which corresponded to the electro-osmotic flow from the anolyte to catholyte. The concentration-driven Na^+ crossover from the catholyte to the anolyte was smaller than the electric-driven K^+ crossover from the anolyte to the catholyte in both TFC and AEM (Figure 5c). Even though Cl^- crossover in the AEM was much larger than in the RO membrane, the net OH^- transport under different conditions was also larger in the AEM (Figure 5d). The net OH^- transport under different conditions with two membranes was calculated based on the fraction of the galvanic current carried by the ion in a pure conduction process in solution. However, in the context of the electrotransport process across a membrane, the transport number is defined as the fraction of the current that is transported by the ion in the membrane with no restriction on its transport mechanisms (Figure 5e).[52] Therefore, transport number calculation here based on the other ion crossover results includes the contribution of electric current from all three components of ion diffusion, electromigration, and convection.[53]

Both K^+ and OH^- played an important role in charge transport in the electrolyzer with the TFC-no PET membrane,

https://doi.org/10.1021/acs.est.3c07957
Environ. Sci. Technol. 2024, 58, 1131−1141

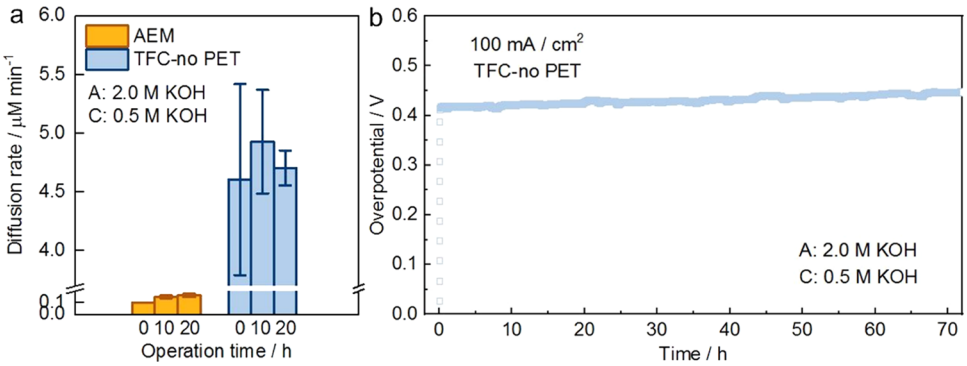

Figure 6. (a) Diffusion rate of 0.5 M NaCl into 0.9 M sucrose solution separated by AEM and TFC-no PET membranes after applying a constant current of 100 mA/cm^2 for different operation time in alkaline electrolytes. (b) Long-term stability of TFC-no PET membrane in 2.0 M KOH analyte and 0.5 M KOH catholyte with an applied constant current density of 100 mA/cm^2 for 72 h without *iR* correction.

while OH^- dominated the charge transport in the electrolyzer with AEM. The higher transport number of OH^- in AEM than TFC-no PET was also consistent with the lower overpotential in the electrolyzer performance test. A much lower rejection of K^+ in the TFC-no PET membrane in the electrolyzer was observed along the direction of the electric field. The difference in ion transport and selectivity during electric field-driven process and pressure-driven process may be attributed to the fundamental distinctions in the driving force of ion transport, the impact of water transport, and the interaction between different ions.[54] The ion transport mechanism of the dense polyamide layer selective and porous support layers in the TFC membrane will be investigated in future studies.

Membrane Stability in AWE. The membrane stability of both AEM and TFC-no PET membranes was examined by measuring the molar rate of salt diffusion through the membranes following AWE operation under different electrolyte conditions at a constant current density of 100 mA/cm^2 at three different times (Figures 6a and S9). The measured salt diffusion rates indicated that the ion rejection of the TFC-no PET membrane was not significantly changed for AWE operation in 0.5 M KOH anolyte and 0.5 M NaCl catholyte (p = 0.74), 2.0 M KOH anolyte and 0.5 M NaCl catholyte (p = 0.66), and 2.0 M KOH anolyte and 0.5 M KOH catholyte (p = 0.80) (Table S2). The diffusion rate was smaller using the AEM than the TFC-no PET membrane (Figure 6a), but the change in time was also not significantly altered by AWE operation (p = 0.20) (Table S2). The stability of the TFC-no PET membrane (2.0 M KOH anolyte and 0.5 M KOH catholyte) for a period longer than experiments conducted here was further confirmed by the highly stable overpotential with a change of only 9.29×10^{-4} V/h over a period of 72 h at a constant current of 100 mA/cm^2 (Figure 6b). The chemical stability of TFC membranes is always a concern for long-term use, which is highly dependent on their polymer composites, and the exposure to conditions out of the specified pH range for a limited period like several weeks appears to be possible.[31,32] Degradation of the active layer can occur at high pH especially at higher temperatures.[32] However, in tests reported here, there was no direct evidence of the chloride rejection decline in performance over time.

The integrity of the polyamide layer of the TFC membrane with an applied pressure was confirmed by dead-end filtration water flux measurements. The permeate flux was quite consistent with a slope of 0.376 ± 0.005 as the hydraulic pressure increased from 5.5 to 35 bar (80−500 psi) (Figure S10). The integrity of the polyamide layer allowed stable operation up to 35 bar (500 psi), suggesting that using the TFC-no PET membrane could enable AWE operation at pressures similar to those of commercial acidic water electrolyzers using proton-exchange membranes (PEMWE, 30−40 bar).[55] In addition, the need for a PET supporting layer is usually only needed for pressures above 80 bar in RO desalination,[37] suggesting that even higher pressures could be sustained using the TFC-no PET membrane that those examined here. Thus, the mechanical stability of the TFC-no PET membrane could enable operation at pressures higher than AWE using traditional porous diaphragms, which are limited to balanced and near-atmospheric pressures.[56,57]

Environmental Implications. With growing concerns over climate change and a significant decline in intermittent renewable electricity costs in recent decades, the production of green hydrogen through water electrolysis presents a promising approach toward achieving a renewable circular economy. Development of cost-effective and energy-efficient water electrolyzers is therefore critical for the implementation of green hydrogen technologies. Despite a slightly higher operation voltage being required for the TFC-no PET membrane compared to the AEM,[58] using the less expensive TFC-no PET (<$10 /m^2) membrane could reduce the AEM costs for AWE ($80 /m^2).[29] More importantly, the use of TFC membranes allows for stable and reliable electrolyzer operation in the presence of impurities in the electrolytes, such as Cl^- ions, without the need for selective OER anode catalysts. Further investigations on the effect of other complex impurities in the natural waters is highly desirable. In addition, the high density of the TFC membrane could enable AWE operation under higher pressures than porous separators which would reduce costs associated with hydrogen gas pressurization. A challenge for AWE operation with the TFC-no PET membrane was an electro-osmotic flow across the membrane when using symmetric electrolytes. However, this was shown to be mitigated with a concentration difference in the electrolytes across the membrane. By using a higher concentration in the anolyte (2 M) and lower concentration in the catholyte (0.5 M), the induced electro-osmotic flow was mitigated and the overpotential was significantly reduced at the set current density. The chemical stability of TFC membranes is highly dependent on their polymer composites, and therefore, changes in these polymers could further improve stability and performance over time. Overall, these results

https://doi.org/10.1021/acs.est.3c07957
Environ. Sci. Technol. 2024, 58, 1131−1141

suggested that TFC membranes are a promising alternative to conventional separators for hydrogen evolution in AWEs. This is because of their fundamentally different structures compared to ion-exchange membranes and their ability to perform well even in the presence of impurities (salts) in the catholyte feed solution. TFC membranes offer the advantages of both porous diaphragms and dense anion-exchange membranes to overcome the trade-off between the ion conductivity and selectivity.

■ ASSOCIATED CONTENT

Supporting Information

The Supporting Information is available free of charge at https://pubs.acs.org/doi/10.1021/acs.est.3c07957.

Photographs of Ni foam-based electrodes, TFC membranes, water electrolyzer setup with the Hg/HgO reference electrode, schematic of a 4-electrode measurement setup, calibration curves of conductivity vs NaCl concentration, LSV measurements for the electrode tested in an alkaline electrolyte with different concentrations, Nyquist plots, calculated diffusion rates of NaCl into sucrose solutions, permeate water flux using the TEC-no PET membrane, osmotic pressure calculations, and statistical analysis summary of ion diffusion rates (PDF)

■ AUTHOR INFORMATION

Corresponding Authors

Le Shi − *Department of Civil and Environmental Engineering, The Pennsylvania State University, University Park, Pennsylvania 16801, United States; College of Environmental and Resource Sciences, Zhejiang University, Hangzhou 310058, P. R. China;* orcid.org/0000-0003-1794-1256; Email: le.shi@zju.edu.cn

Bruce E. Logan − *Department of Civil and Environmental Engineering, The Pennsylvania State University, University Park, Pennsylvania 16801, United States; Department of Chemical Engineering, The Pennsylvania State University, University Park, Pennsylvania 16801, United States;* orcid.org/0000-0001-7478-8070; Phone: +1-814-863-7908; Email: blogan@psu.edu

Authors

Xuechen Zhou − *Department of Civil and Environmental Engineering, The Pennsylvania State University, University Park, Pennsylvania 16801, United States;* orcid.org/0000-0001-8007-4787

Rachel F. Taylor − *Department of Chemical Engineering, The Pennsylvania State University, University Park, Pennsylvania 16801, United States;* orcid.org/0000-0002-2576-8193

Chenghan Xie − *Department of Civil and Environmental Engineering, The Pennsylvania State University, University Park, Pennsylvania 16801, United States;* orcid.org/0000-0002-4962-9737

Bin Bian − *Department of Civil and Environmental Engineering, The Pennsylvania State University, University Park, Pennsylvania 16801, United States;* orcid.org/0000-0001-5270-4964

Derek M. Hall − *Department of Mechanical Engineering, The Pennsylvania State University, University Park, Pennsylvania 16801, United States;* orcid.org/0000-0001-9648-596X

Ruggero Rossi − *Department of Civil and Environmental Engineering, The Pennsylvania State University, University Park, Pennsylvania 16801, United States; Department of Environmental Health and Engineering, Johns Hopkins University, Baltimore, Maryland 21218, United States;* orcid.org/0000-0002-3807-3980

Michael A. Hickner − *Department of Materials Science and Engineering, The Pennsylvania State University, University Park, Pennsylvania 16801, United States;* orcid.org/0000-0002-2252-7626

Christopher A. Gorski − *Department of Civil and Environmental Engineering, The Pennsylvania State University, University Park, Pennsylvania 16801, United States;* orcid.org/0000-0002-5363-2904

Complete contact information is available at: https://pubs.acs.org/10.1021/acs.est.3c07957

Notes

The authors declare no competing financial interest.

■ ACKNOWLEDGMENTS

The authors acknowledge funding by Penn State University and the National Science Foundation CBET-2027552. The authors thank Arash Emdadi and Michael Geitner from the Department of Chemical Engineering at PSU for helping with the EIS and dead-end filtration tests.

■ REFERENCES

(1) Shi, Y.; Zhang, B. Recent advances in transition metal phosphide nanomaterials: synthesis and applications in hydrogen evolution reaction. *Chem. Soc. Rev.* **2016**, *45* (6), 1529−1541.

(2) Stolten, D. *Hydrogen and Fuel Cells: Fundamentals, Technologies and Applications*; John Wiley & Sons, 2010.

(3) Kraglund, M. R.; Carmo, M.; Schiller, G.; Ansar, S. A.; Aili, D.; Christensen, E.; Jensen, J. O. Ion-solvating membranes as a new approach towards high rate alkaline electrolyzers. *Energy Environ. Sci.* **2019**, *12* (11), 3313−3318 10.1039/C9EE00832B.

(4) Anantharaj, S.; Aravindan, V. Developments and Perspectives in 3d Transition-Metal-Based Electrocatalysts for Neutral and Near-Neutral Water Electrolysis. *Adv. Energy Mater.* **2020**, *10* (1), No. 1902666.

(5) Chatenet, M.; Pollet, B. G.; Dekel, D. R.; Dionigi, F.; Deseure, J.; Millet, P.; Braatz, R. D.; Bazant, M. Z.; Eikerling, M.; Staffell, I.; Balcombe, P.; Shao-Horn, Y.; Schäfer, H. Water electrolysis: from textbook knowledge to the latest scientific strategies and industrial developments. *Chem. Soc. Rev.* **2022**, *51* (11), 4583−4762 10.1039/D0CS01079K.

(6) Birol, F. The future of hydrogen: seizing today's opportunities *IEA Report prepared for the G* 2019; Vol. *20*.

(7) Logan, B. E.; Shi, L.; Rossi, R. Enabling the use of seawater for hydrogen gas production in water electrolyzers. *Joule* **2021**, *5* (4), 760−762.

(8) Mayyas, A. T.; Ruth, M. F.; Pivovar, B. S.; Bender, G.; Wipke, K. B. *Manufacturing Cost Analysis for Proton Exchange Membrane Water Electrolyzers*; National Renewable Energy Lab.(NREL): Golden, CO (United States), 2019.

(9) Esposito, D. V. Membraneless electrolyzers for low-cost hydrogen production in a renewable energy future. *Joule* **2017**, *1* (4), 651−658.

(10) Xiang, C.; Papadantonakis, K. M.; Lewis, N. S. Principles and implementations of electrolysis systems for water splitting. *Mater. Horiz.* **2016**, *3* (3), 169−173 10.1039/C6MH00016A.

(11) Patel, S. K.; Biesheuvel, P. M.; Elimelech, M. Energy Consumption of Brackish Water Desalination: Identifying the Sweet Spots for Electrodialysis and Reverse Osmosis. *ACS ES&T Engg* **2021**, *1* (5), 851−864.

(12) Fahad Aldosari, O.; Hussain, I.; Malaibari, Z. Emerging trends of electrocatalytic technologies for renewable hydrogen energy from seawater: Recent advances, challenges, and techno-feasible assessment. *J. Energy Chem.* **2023**, *80*, 658−688.
(13) Karagiannis, I. C.; Soldatos, P. G. Water desalination cost literature: review and assessment. *Desalination* **2008**, *223* (1), 448−456.
(14) Hausmann, J. N.; Schlögl, R.; Menezes, P. W.; Driess, M. Is direct seawater splitting economically meaningful? *Energy Environ. Sci.* **2021**, *14* (7), 3679−3685 10.1039/D0EE03659E.
(15) Veroneau, S. S.; Nocera, D. G. Continuous electrochemical water splitting from natural water sources via forward osmosis. *Proc. Natl. Acad. Sci. U.S.A.* **2021**, *118* (9), No. e2024855118.
(16) Schalenbach, M.; Zeradjanin, A. R.; Kasian, O.; Cherevko, S.; Mayrhofer, K. J. A perspective on low-temperature water electrolysis−challenges in alkaline and acidic technology. *Int. J. Electrochem. Sci.* **2018**, *13* (2), 1173−1226.
(17) Zeng, K.; Zhang, D. Recent progress in alkaline water electrolysis for hydrogen production and applications. *Prog. Energy Combust. Sci.* **2010**, *36* (3), 307−326.
(18) Schmidt, O.; Gambhir, A.; Staffell, I.; Hawkes, A.; Nelson, J.; Few, S. Future cost and performance of water electrolysis: An expert elicitation study. *Int. J. Hydrogen Energy* **2017**, *42* (52), 30470−30492.
(19) Miller, H. A.; Bouzek, K.; Hnat, J.; Loos, S.; Bernäcker, C. I.; Weißgärber, T.; Röntzsch, L.; Meier-Haack, J. Green hydrogen from anion exchange membrane water electrolysis: a review of recent developments in critical materials and operating conditions. *Sustainable Energy Fuels* **2020**, *4* (5), 2114−2133 10.1039/C9SE01240K.
(20) Tong, W.; Forster, M.; Dionigi, F.; Dresp, S.; Sadeghi Erami, R.; Strasser, P.; Cowan, A. J.; Farràs, P. Electrolysis of low-grade and saline surface water. *Nat. Energy* **2020**, *5* (5), 367−377.
(21) Liu, Z.; Sajjad, S. D.; Gao, Y.; Yang, H.; Kaczur, J. J.; Masel, R. I. The effect of membrane on an alkaline water electrolyzer. *Int. J. Hydrogen Energy* **2017**, *42* (50), 29661−29665.
(22) Carmo, M.; Fritz, D. L.; Mergel, J.; Stolten, D. A comprehensive review on PEM water electrolysis. *Int. J. Hydrogen Energy* **2013**, *38* (12), 4901−4934.
(23) Schalenbach, M.; Lueke, W.; Stolten, D. Hydrogen diffusivity and electrolyte permeability of the Zirfon PERL separator for alkaline water electrolysis. *J. Electrochem. Soc.* **2016**, *163* (14), F1480.
(24) Ahmad Kamaroddin, M. F.; Sabli, N.; Tuan Abdullah, T. A.; Siajam, S. I.; Abdullah, L. C.; Abdul Jalil, A.; Ahmad, A. Membrane-Based Electrolysis for Hydrogen Production: A Review. *Membranes* **2021**, *11* (11), 810.
(25) Li, D.; Motz, A. R.; Bae, C.; Fujimoto, C.; Yang, G.; Zhang, F.-Y.; Ayers, K. E.; Kim, Y. S. Durability of anion exchange membrane water electrolyzers. *Energy Environ. Sci.* **2021**, *14* (6), 3393−3419 10.1039/D0EE04086J.
(26) Rossi, R.; Taylor, R.; Logan, B. E. Increasing the Electrolyte Salinity to Improve the Performance of Anion Exchange Membrane Water Electrolyzers. *ACS Sustainable Chem. Eng.* **2023**, *11*, 8573.
(27) Dai, Q.; Liu, Z.; Huang, L.; Wang, C.; Zhao, Y.; Fu, Q.; Zheng, A.; Zhang, H.; Li, X. Thin-film composite membrane breaking the trade-off between conductivity and selectivity for a flow battery. *Nat. Commun.* **2020**, *11* (1), No. 13, DOI: 10.1038/s41467-019-13704-2.
(28) Alam, A.; Park, C.; Lee, J.; Ju, H. Comparative analysis of performance of alkaline water electrolyzer by using porous separator and ion-solvating polybenzimidazole membrane. *Renewable Energy* **2020**, *166*, 222−233.
(29) Shi, L.; Rossi, R.; Son, M.; Hall, D. M.; Hickner, M. A.; Gorski, C. A.; Logan, B. E. Using reverse osmosis membranes to control ion transport during water electrolysis. *Energy Environ. Sci.* **2020**, *13* (9), 3138−3148 10.1039/D0EE02173C.
(30) Taylor, R.; Shi, L.; Zhou, X.; Rossi, R.; Picioreanu, C.; Logan, B. E. Electrochemical and hydraulic analysis of thin-film composite and cellulose triacetate membranes for seawater electrolysis applications. *J. Membr. Sci.* **2023**, *679*, No. 121692.
(31) Chai, Y. K.; Lam, H. C.; Koo, C. H.; Lau, W. J.; Lai, S. O.; Ismail, A. F. Performance evaluation of polyamide nanofiltration membranes for phosphorus removal process and their stability against strong acid/alkali solution. *Chin. J. Chem. Eng.* **2019**, *27* (8), 1789−1797.
(32) Bargeman, G. Recent developments in the preparation of improved nanofiltration membranes for extreme pH conditions. *Sep. Purif. Technol.* **2021**, *279*, No. 119725.
(33) Gu, K.; Wang, K.; Zhou, Y.; Gao, C. Alkali-resistant polyethyleneimine/triglycidyl isocyanurate nanofiltration membrane for treating lignin lye. *J. Membr. Sci.* **2021**, *637*, No. 119631.
(34) Yu, L.; Zhu, Q.; Song, S.; McElhenny, B.; Wang, D.; Wu, C.; Qin, Z.; Bao, J.; Yu, Y.; Chen, S.; Ren, Z. Non-noble metal-nitride based electrocatalysts for high-performance alkaline seawater electrolysis. *Nat. Commun.* **2019**, *10* (1), No. 5106, DOI: 10.1038/s41467-019-13092-7.
(35) Yu, L.; Wu, L.; McElhenny, B.; Song, S.; Luo, D.; Zhang, F.; Yu, Y.; Chen, S.; Ren, Z. Ultrafast room-temperature synthesis of porous S-doped Ni/Fe (oxy)hydroxide electrodes for oxygen evolution catalysis in seawater splitting. *Energy Environ. Sci.* **2020**, *13* (10), 3439−3446 10.1039/D0EE00921K.
(36) Naito, T.; Shinagawa, T.; Nishimoto, T.; Takanabe, K. Water Electrolysis in Saturated Phosphate Buffer at Neutral pH. *ChemSusChem* **2020**, *13* (22), 5921−5933.
(37) Davenport, D. M.; Deshmukh, A.; Werber, J. R.; Elimelech, M. High-Pressure Reverse Osmosis for Energy-Efficient Hypersaline Brine Desalination: Current Status, Design Considerations, and Research Needs. *Environ. Sci. Technol. Lett.* **2018**, *5* (8), 467−475.
(38) Wang, X.; Rossi, R.; Yan, Z.; Yang, W.; Hickner, M. A.; Mallouk, T. E.; Logan, B. E. Balancing Water Dissociation and Current Densities To Enable Sustainable Hydrogen Production with Bipolar Membranes in Microbial Electrolysis Cells. *Environ. Sci. Technol.* **2019**, *53* (24), 14761−14768.
(39) Dresp, S.; Dionigi, F.; Loos, S.; Ferreira de Araujo, J.; Spöri, C.; Gliech, M.; Dau, H.; Strasser, P. Direct Electrolytic Splitting of Seawater: Activity, Selectivity, Degradation, and Recovery Studied from the Molecular Catalyst Structure to the Electrolyzer Cell Level. *Adv. Energy Mater.* **2018**, *8* (22), No. 1800338.
(40) Fontananova, E.; Zhang, W.; Nicotera, I.; Simari, C.; van Baak, W.; Di Profio, G.; Curcio, E.; Drioli, E. Probing membrane and interface properties in concentrated electrolyte solutions. *J. Membr. Sci.* **2014**, *459*, 177−189.
(41) Haverkort, J. W.; Rajaei, H. Voltage losses in zero-gap alkaline water electrolysis. *J. Power Sources* **2021**, *497*, No. 229864.
(42) Vilanova, A.; Dias, P.; Azevedo, J.; Wullenkord, M.; Spenke, C.; Lopes, T.; Mendes, A. Solar water splitting under natural concentrated sunlight using a 200 cm2 photoelectrochemical-photovoltaic device. *J. Power Sources* **2020**, *454*, No. 227890.
(43) Zhao, Y.; Duan, L. Research on Measuring Pure Membrane Electrical Resistance under the Effects of Salinity Gradients and Diffusion Boundary Layer and Double Layer Resistances. *Membranes* **2022**, *12* (8), 816.
(44) Bohinc, K.; Kralj-Iglič, V.; Iglič, A. Thickness of electrical double layer. Effect of ion size. *Electrochim. Acta* **2001**, *46* (19), 3033−3040.
(45) Sheng, W.; Zhuang, Z.; Gao, M.; Zheng, J.; Chen, J. G.; Yan, Y. Correlating hydrogen oxidation and evolution activity on platinum at different pH with measured hydrogen binding energy. *Nat. Commun.* **2015**, *6* (1), No. 5848, DOI: 10.1038/ncomms6848.
(46) Wang, X.; Xu, C.; Jaroniec, M.; Zheng, Y.; Qiao, S.-Z. Anomalous hydrogen evolution behavior in high-pH environment induced by locally generated hydronium ions. *Nat. Commun.* **2019**, *10* (1), No. 4876, DOI: 10.1038/s41467-019-12773-7.
(47) Iwata, R.; Zhang, L.; Wilke, K. L.; Gong, S.; He, M.; Gallant, B. M.; Wang, E. N. Bubble growth and departure modes on wettable/non-wettable porous foams in alkaline water splitting. *Joule* **2021**, *5* (4), 887−900.

(48) Haverkort, J. W.; Rajaei, H. Electro-osmotic flow and the limiting current in alkaline water electrolysis. *J. Power Sources Adv.* **2020**, *6*, No. 100034.
(49) Dydek, E. V.; Zaltzman, B.; Rubinstein, I.; Deng, D. S.; Mani, A.; Bazant, M. Z. Overlimiting Current in a Microchannel. *Phys. Rev. Lett.* **2011**, *107* (11), No. 118301, DOI: 10.1103/PhysRevLett.107.118301.
(50) Nikonenko, V. V.; Lebedev, K. A.; Suleimanov, S. S. Influence of the convective term in the Nernst-Planck equation on properties of ion transport through a layer of solution or membrane. *Russ. J. Electrochem.* **2009**, *45* (2), 160−169 Article.
(51) Haverkort, J. W. Modeling and Experiments of Binary Electrolytes in the Presence of Diffusion, Migration, and Electro-Osmotic Flow. *Phys. Rev. Appl.* **2020**, *14* (4), No. 044047.
(52) Sorenson, T. S. *Surface Chemistry and Electrochemistry of Membranes*; CRC Press, 1999.
(53) Zhou, X.; Shi, L.; Taylor, R. F.; Xie, C.; Bian, B.; Picioreanu, C.; Logan, B. E. Relative Insignificance of Polyamide Layer Selectivity for Seawater Electrolysis Applications. *Environ. Sci. Technol.* **2023**, *57*, 14569.
(54) Wang, R.; Zhang, J.; Tang, C. Y.; Lin, S. Understanding Selectivity in Solute−Solute Separation: Definitions, Measurements, and Comparability. *Environ. Sci. Technol.* **2022**, *56* (4), 2605−2616.
(55) Ayers, K. E.; Anderson, E. B.; Capuano, C.; Carter, B.; Dalton, L.; Hanlon, G.; Manco, J.; Niedzwiecki, M. Research Advances towards Low Cost, High Efficiency PEM Electrolysis. *ECS Trans.* **2010**, *33* (1), 3.
(56) Schalenbach, M.; Tjarks, G.; Carmo, M.; Lueke, W.; Mueller, M.; Stolten, D. Acidic or Alkaline? Towards a New Perspective on the Efficiency of Water Electrolysis. *J. Electrochem. Soc.* **2016**, *163* (11), F3197.
(57) Hancke, R.; Holm, T.; Ulleberg, Ø. The case for high-pressure PEM water electrolysis. *Energy Convers. Manage.* **2022**, *261*, No. 115642.
(58) Omosebi, A.; Gao, X.; Holubowitch, N.; Li, Z.; Landon, J.; Liu, K. Anion Exchange Membrane Capacitive Deionization Cells. *J. Electrochem. Soc.* **2017**, *164* (9), No. E242.

https://doi.org/10.1021/acs.est.3c07957
Environ. Sci. Technol. 2024, 58, 1131−1141